Spin-label EPR on Disordered and Amyloid Proteins

Hashemi Shabestari, M.

CHAPTER 5

ELUCIDATING THE α-SYNUCLEIN FIBRIL FOLD WITH PULSED EPR

Amyloid fibrils are constituents of the plaques that are the hallmarks of neurodegenerative diseases. In Parkinson's disease, these plaques (Lewy bodies) consist predominantly of the α-synuclein (αS) protein. To understand how the aggregation occurs and to interfere with the process of aggregation, the structure of the fibrils needs to be known. Here we study the molecular architecture of the fibrils of αS by measuring distances between pairs of residues in the protein using double electron-electron paramagnetic resonance (DEER). Site-specific spin labeling was employed to create nine doubly labeled αS variants, which were investigated in the fibrillar state. Diamagnetic dilution with wild type αS suppressed inter-molecular interactions. The intra-molecular distances provide constraints for the fold of the protein inside the fibril. Intra-molecular distances were unambiguously determined for four pairs 41/69, 56/69, 56/90, and 69/90. Three of these distances provide the constraints to suggest a model for the fold between residues 56 and 90 in the fibril.

Maryam Hashemi Shabestari, Ine M.J. Segers-Nolten, Mireille M.A.E. Claessens, Bart D. van Rooijen, Vinod Subramaniam, Martina Huber.

5.1 Introduction

Alpha-synuclein (αS) is a protein of 140 amino-acid residues. The αS protein is implicated in Parkinson's disease and is the major component of the Lewy Bodies characteristic of Parkinson's disease [1]. The αS protein is natively disordered with no distinct secondary structure in solution. It acquires an α-helical structure on membranes. When αS forms fibrils, individual β-strands stack perpendicular to the fibril axis and form a cross β-sheet structure [2,3]. It is important to understand the architecture of the fibril and to identify the residues that are crucial for the fibrillization. As yet, detailed information about the structure and fold of the protein in the fibrils is missing. Results from solid state NMR and EPR studies have identified residues involved in the β-sheet [4,5] and proposals for the fold of stretches of residues in close contact were made [6,7]. Owing to the absence of long-range constraints, modeling the exact extent of the stretches is difficult. In this work, we focus on the fold of αS in the fibril, by measuring intra-molecular distances in fibrillized doubly labeled αS with a pulsed EPR method, DEER. Recently, distance constraints involving residues located at the external β-strands were reported using the same approach [8].

We investigate nine doubly labeled αS variants, αS9/69, αS9/90, αS18/69, αS18/90, αS27/56, αS41/69, αS56/69, αS56/90, and αS69/90. From the set of nine mutants, four, αS41/69, αS56/69, αS56/90, and αS69/90, have intra-molecular distances within the measurement range of the experiment. Based on the DEER distance data and combined with a triangulation approach, we construct a model of the fold of αS in the fibril using a set of three intra-molecular distances: αS56/69, αS56/90, and αS69/90.

The present study shows that even for such challenging repetitive protein structures a few long-distance constraints from DEER experiments are sufficient to obtain structural detail of fibrils that comprises most of the strands considered in the present models.

5.2 Materials and methods

5.2.1 Expression and purification of cysteine variants of αS

Single and double cysteine mutations were introduced into the αS gene by site directed mutagenesis. Mutants were expressed in *Escherichia coli* strain BL21(DE3) and subsequently purified in the presence of 1 mM DL-Dithiothreitol (DTT) [9,10]. Prior to labeling, αS mutant proteins were reduced with a six-fold molar excess (per cysteine) of DTT for 30 minutes at room temperature. Subsequently, samples were desalted on Pierce Zeba 5 mL desalting columns,

followed by an immediate addition of a six-fold molar excess (per cysteine) of the MTS spin label ((1-oxyl-2,2,5,5-tetramethylpyrroline-3-methyl) methanethiosulfonate) and incubated for one hour in the dark at room temperature. Free label was removed using two additional desalting steps. Protein samples were applied onto Microcon YM-100 spin columns to remove any precipitated and/or oligomerized proteins and diluted into 10 mM Tris-HCl, pH 7.4 to typical protein concentrations of approximately 0.25 mM [11].

5.2.2 Preparation and harvesting of fibrillar αS

Fibrils of αS were formed by incubating monomer solutions at a total protein concentration of 100 μM. Due to the stacking of proteins along the fibril axis, discrimination between intra- and inter-molecular distances is necessary. Therefore, the spin-labeled variants were co-fibrillized with the wild type αS protein (diamagnetic dilution). Different diamagnetic dilution ratios ranging from 1 in 5 to 1 in 20 were employed to ensure that the obtained distances represent the intramolecular distances. Fibrils of all mutants were prepared using a diamagnetic dilution of 10 μM MTS labeled αS (SL-αS) in the presence of 90 μM wild type αS (1 in 10). For selected mutants, fibrillization of the double cysteine mutants was carried out in a 1 in 20 diamagnetic dilution, using 5 μM doubly labeled SL-αS together with 95 μM wild type protein. The corresponding single cysteine mutants were fibrillized in a 1 in 10 ratio, to keep the spin-label concentrations comparable. For the diamagnetic dilution series, fibrils were prepared with 20 μM αS56/69 and 80 μM wild type (1 in 5), 10 μM αS56/69 and 90 μM wild type (1 in 10) and 5 μM αS56/69 and 95 μM wild type (1 in 20). The aggregations were performed in 10 mM Tris-HCl, 50 mM NaCl, pH 7.4 buffer at 37° C in 2 ml LoBind Eppendorf tubes with constant shaking at 1000 rpm in a Thermo mixer (Eppendorf). The time evolution of αS aggregation was monitored by the standard Thioflavin T (ThioT) fluorescence assay [12,13]. The fibrillization was generally completed in three to four days. The αS fibrils were harvested by centrifuging for 90 minutes at 18,000 g in an Eppendorf microcentrifuge. The supernatant was carefully removed, leaving a fibril pellet typically with a volume of 80-100 μl. The fibril pellet was used in the cw EPR and DEER measurements. Every mutant was fibrillized at least two times.

5.2.3 Atomic force microscopy (AFM)

The formation of αS fibrils was confirmed by tapping mode AFM in air. Aggregation aliquots were diluted in 10 mM Tris, 50 mM NaCl, pH 7.4, adsorbed onto mica, washed twice with 100 μl MilliQ water and gently dried under nitrogen gas. Tapping mode AFM height images were made on a custom built instrument

[9,14]. SPIP software (Image Metrology A/S, Lyngby, Denmark) was used for visualization.

5.2.4 Continuous-wave EPR at 80 K and at room temperature

The X-band cw EPR measurements were performed using an Elexys E680 spectrometer (Bruker, Rheinstetten, Germany) with a rectangular cavity, using a modulation frequency of 100 kHz. For measurements at 80 K a helium gas-flow cryostat (Oxford Instruments, United Kingdom) with an ITC502 temperature controller (Oxford Instruments, United Kingdom) was used. For the measurements in frozen solution, 3 mm outer diameter quartz sample tubes were used. To obtain a frozen glass 20 % glycerol was added to the samples before freezing them in liquid nitrogen. The frozen samples were inserted in the pre-cooled helium gas-flow cryostat. The EPR spectra were recorded using a modulation amplitude of 2 G and a microwave power of 0.159 mW. Typical accumulation times were 40 minutes. For room temperature measurements, 10-15 µl samples of αS fibrils were drawn into Blaubrand 50 µl capillaries. The accumulation time for the spectra was 40 minutes per spectrum. Measurements were done at 20° C, using 6.331 mW of microwave power and a modulation amplitude of 1.4 G.

5.2.5 DEER measurements

The DEER measurements were performed at X-band (9.5 GHz) on an Elexsys E680 spectrometer (Bruker, Rheinstetten, Germany) using a 3 mm split-ring resonator (ER 4118XMS-3-W1). The temperature was kept at 40 K with a helium gas stream using a CF935 (Oxford Instruments, United Kingdom) cryostat with an ITC502 temperature controller (Oxford Instruments, United Kingdom). Samples, to which 20 % glycerol was added, were prepared in 3 mm outer diameter quartz tubes and were frozen in liquid nitrogen before inserting them into pre-cooled helium gas-flow cryostat. The pump and observer frequencies were separated by 70 MHz and adjusted as reported before [11]. The pump-pulse power was adjusted to invert the echo maximally [15]. The lengths of the pulses at the observer frequencies were 16 and 32 ns for π/2- and π-pulses, respectively. The pump pulse length was 12 ns. All the DEER measurements were performed as two-dimensional experiments, in order to suppress the proton modulation. The DEER time traces were measured for ten different τ_1-values spaced by 8 ns starting at τ_1 = 200 ns. The typical accumulation times per sample were 16 hours. DEER data were analyzed using the "DeerAnalysis" program 2011 [16], which is available from www.epr.ethz.ch/software/index. After background correction of the data using the experimental background,

obtained from the singly labeled αS samples, the distance distribution was determined by Tikhonov regularization [15,16].

5.2.6 General structure parameters of fibrils

Generally accepted parameters [17] of the parallel β-sheet architecture of amyloid fibrils are the intra-sheet distance *d* of 1.09 nm, and the distance between two neighbors in the sequence within a strand *l* of 0.35 nm [17] (see results). From the distance *l* and the number of intervening residues between a pair of spin labeled residues, the distance expected between two labeled residues on the same strand was determined. For the model of the fibril, three orientations of the linker were considered per residue, each 120° apart with the linker in the same plane as the protein. Nine unique relative linker orientations are possible in that case.

5.3 Results

We have investigated nine doubly labeled αS variants, αS9/69, αS35/60, αS18/69, αS18/90, αS27/56, αS41/69, αS56/69, αS56/90, and αS69/90. These proteins are fibrillized in the presence of wild type αS (diamagnetic dilution) under the conditions explained in materials and methods.
The rate of formation of the αS fibrils is checked by the thioflavin T fluorescence assay [12,13]. No significant difference in the rate of fibril formation is observed for all samples, irrespective of the spin-label position and the degree of diamagnetic dilution. The morphology of the fibrils is checked by atomic force microscopy (AFM). As seen by AFM (figure 5.1) the morphology of the wild type and the spin-labeled mutants is similar, revealing that the spin label does not affect the fibrillization. The αS fibrils are investigated with continuous-wave and pulsed EPR.

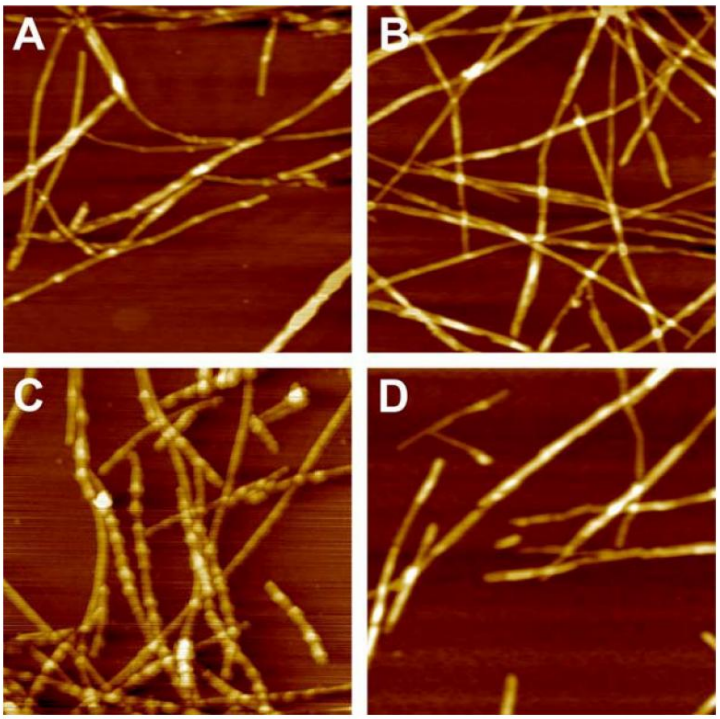

Figure 5.1 AFM images (A-D) of fibrils. A: αS56, at diamagnetic dilution 1 in 20, B: αS56/69 at 1 in 10, C: αS56/90 at 1 in 10, D: αS69/90 at 1 in 20. All images are 2.5 x 2.5 μm^2. Height information is rendered by the density of the color. Range: 0 to 10 nm.

5.3.1 Continuous-wave EPR

The continuous wave EPR spectra of the harvested fibrils of the αS56/69, αS56/90, and αS69/90 mutants with their singly labeled counterparts, αS56, αS69, and αS90 in liquid solution (left) and in frozen solution (right) are shown in figure 5.2. The liquid solution spectra have broadened lines with respect to those of the non-fibrillized αS protein. Simulation shows that the line-shape is fully explained by a reduced mobility of the spin label. This indicates that the broadening is caused by partial immobilization of the spin label due to fibrillization rather than spin-spin interaction. The narrow lines marked in figure 5.2 are indicative of the presence of monomers in the fibril sample. According to the simulation, the harvested fibrils contain less than 10 % of non-fibrillized protein.

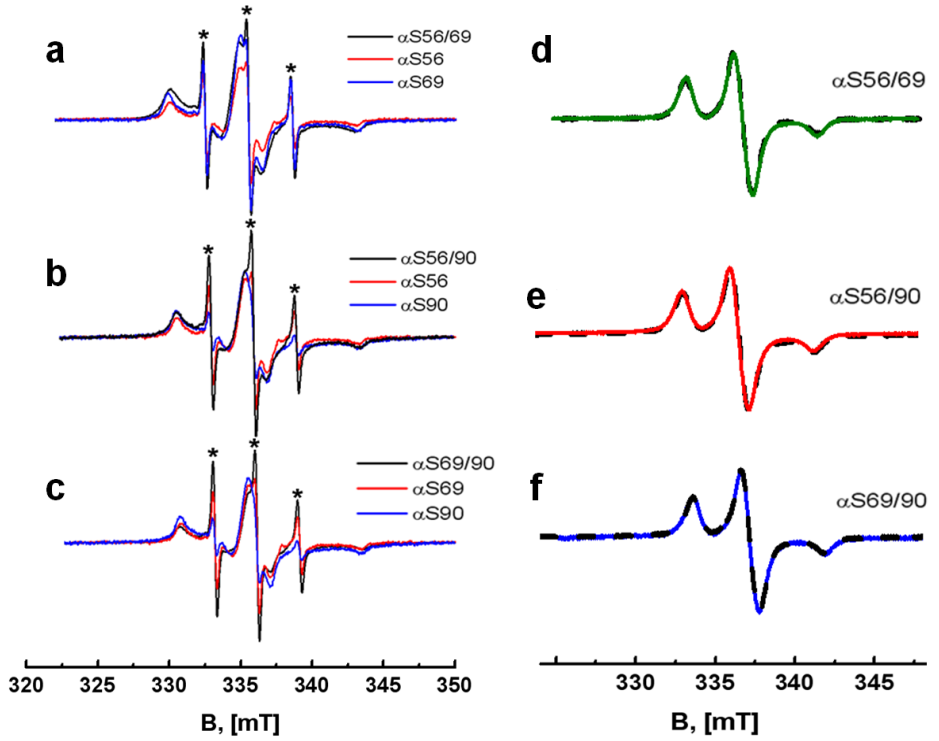

Figure 5.2 Continuous wave EPR spectra of the harvested fibrils of αS in a 1 in 10 diamagnetic dilution. a to c: Room temperature spectra of fibrils of doubly labeled αS with the corresponding singly labeled counterparts. Narrow lines, marked by an asterisk, stem from a small (less than 10 %) contribution of non-fibrillized proteins. a: αS56/69 superimposed with αS56 and αS69, b: αS56/90 superimposed with αS56 and αS90, c: αS69/90 superimposed with αS69 and αS90. d to f: Frozen solution EPR spectra of the doubly labeled αS proteins with the 1:1 added spectra of the respective singly labeled counterparts. d: αS56/69 (green) superimposed with αS56 plus αS69 (black), e: αS56/90 (red) superimposed with αS56 plus αS90 (black), f: αS69/90 (blue) superimposed with αS69 plus αS90 (black).

Frozen solution cw EPR spectra are superimposed with the 1:1 added spectra of the respective singly labeled counterparts. The absence of line broadening in the frozen solution spectra of the samples of fibrils with doubly labeled proteins compared to those of the singly labeled samples is evidence for the absence of distances shorter than 1.5 nm [4,5].

5.3.2 Pulsed EPR

The DEER time traces of all mutants are shown in figure 5.3. The DEER time traces of αS9/69, αS18/69, and αS18/90 have a shallow decay, i.e., small modulation depth, which is an indication that a large fraction of the population has distances outside the measurement range, i.e., shorter than 1.8 nm or longer than 5

nm. The absence of line broadening in frozen solution, cw EPR shows that there are no distances shorter than 1.5 nm. Therefore, the majority of the population with distances outside the measurement range must have distances longer than 5 nm. The DEER time traces of the other mutants have a larger modulation depth. Some of those traces show signatures of DEER modulation, for example the steep decay at about 0.35 µs for αS56/69.

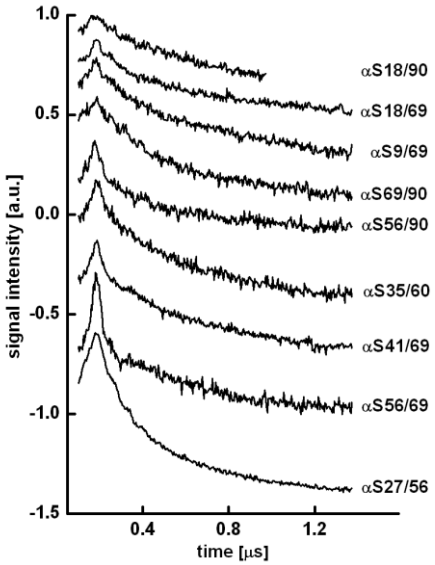

Figure 5.3 The DEER time traces for αS18/90, αS18/69, αS9/69, αS69/90, αS56/90, αS35/60, αS41/69, αS56/69, and αS27/56. All samples are in a 1 in 10 (spin-labeled αS in total αS) diamagnetic dilution, except for the αS35/60 mutant in which the dilution is 1 in 20. The maximum intensity of the DEER traces is normalized to one, by dividing the trace by the maximum of its intensity. DEER time traces are vertically shifted with respect to each other for better visibility.

Of the mutants analyzed, we focus the description on those with a large modulation depth, mutants αS56/69, αS56/90, αS69/90, and αS41/69. The αS18/69 is used as a reference for the mutants with low modulation depth. Figure 5.4 shows the steps in the analysis of the DEER time traces. All traces are background corrected with a 1:1 ratio of the background derived from the DEER curves of the respective singly labeled αS variants, which were fibrillized under the same conditions as the doubly labeled counterparts (for details see figure caption). Distances below 2 nm cannot be reliably determined under the conditions of the DEER experiments [18].

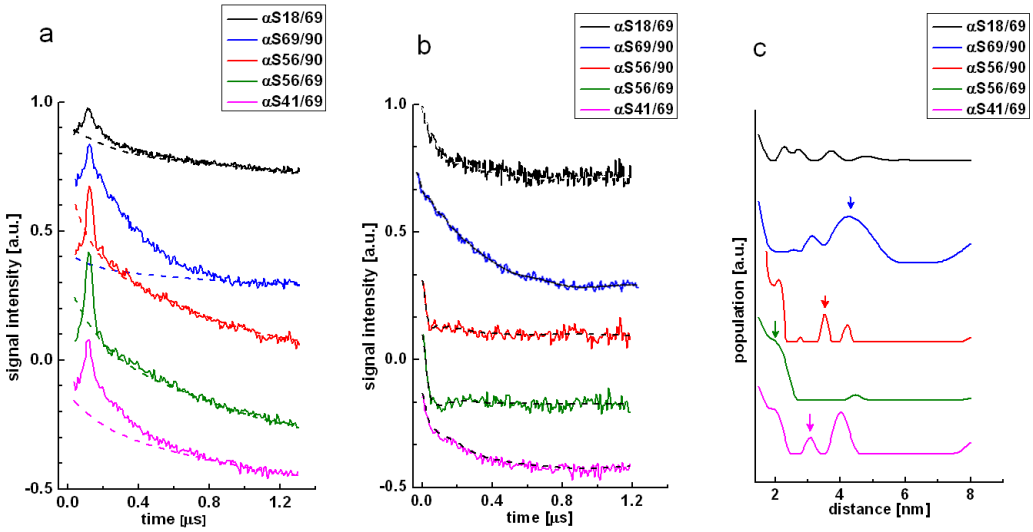

Figure 5.4 The DEER time traces for mutants αS18/69, αS69/90, αS56/90, αS56/69, and αS41/69. Shown are: a: DEER time traces. The background is shown as a dotted line. Backgrounds are the 1:1 added background traces of fibrils of the respective singly labeled αS. The background correction is done by dividing the data by the experimental background. Spin-label dilutions are 1 in 20 (spin-labeled αS in total αS) except for αS18/69 and αS41/69, which are 1 in 10. The maximum intensity of the DEER time traces is normalized to 1 and the traces are vertically shifted for better visibility. b: Baseline corrected DEER time traces and fit of the modulations to the data corresponding to the distance distributions shown in c. c: Distance distributions derived from the data. Arrows mark the distances identified as intra-molecular distances. Distributions were individually scaled to improve visibility.

To discriminate between intra- and inter-molecular distances, a set of diamagnetic dilutions is measured for the αS56/69 mutant (figure 5.5). The relative intensity of the peaks at 2.7 nm, 3.9 nm, and 4.5 nm compared to the 2.1 nm distance peak diminishes with increasing diamagnetic dilution, showing that the former peaks are due to inter-molecular interactions. These inter-molecular peaks are also found in the distance distributions of the corresponding singly labeled mutants, which confirm the inter-molecular character of these distances. As outlined below (see discussion) the intermolecular interactions should be independent of the mutant. Therefore, the inter-molecular distances identified for αS56/69 are also used in the interpretation of the distance distributions of the other mutants. Considering the signal-to-noise ratio of the time traces for the diamagnetic dilution of 1:20, higher dilutions do not seem feasible. The first screen of all mutants was performed at a 1:10 dilution to obtain a good signal-to-noise ratio. For selected mutants, αS56/69,

αS56/90, and αS69/90 the measurements were repeated at 1 in 20 dilution to improve the discrimination of intra- and inter-molecular distances.

Table 5.1 Distances from DEER experiments in nm compared to the expected distances for residues on the same β-strand.

mutants	intra-molecular DEER distances	distances expected for residues on the same β-strand
αS56/69	2.1	4.5
αS56/90	3.4	11.9
αS69/90	≥ 4.0	7.3
αS41/69	3.1	9.8

Figure 5.4.c shows the distance distributions for the mutants analyzed in detail. Intra-molecular distances are marked as arrows in figure 5.4.c. The αS18/69 mutant shows distances with similar intensities all over the accessible distance range. The same is true for αS27/56 (data not shown). The αS69/90 mutant shows two peaks, one around 2.6 nm and one around 4.2 nm. The second peak of the αS69/90 mutant corresponds to a larger population than the first peak. The αS56/90 mutant has a contribution at short distances (≤ 2.5 nm) that is very similar to the inter-molecular contribution in figure 5.5. The same is true for the lower intensity peak at 4 nm. This leaves the peak at 3.4 nm as an intra-molecular distance. The αS56/69 mutant shows a dominant distance peak around 2 nm, which is intra-molecular (see above). The αS41/69 mutant, which was fibrillized at a 1 in 10 diamagnetic dilution ratio, shows three peaks: one at distances longer than 4 nm, one around 2 nm, and one around 3 nm. The distance peaks at 2 nm and 4 nm are close to inter-molecular distance peaks as observed for αS56/69 at 1 in 10 diamagnetic dilution (figure 5.5). We therefore consider only the distance peak at 3 nm as intra-molecular. The αS27/56 mutant (with 1 in 10 diamagnetic dilution, data not shown) has a broad continuous distance distribution from 2 to 4 nm.

The intra-molecular distances are collected in table 5.1. They are compared to expected distances for residues on the same strand, which are calculated from the distance between two neighbors in the sequence within a strand, l [17] and the number of intervening residues (see materials and methods). The distances determined for all mutants listed in table 5.1 are shorter than the distances expected for residues on the same strand.

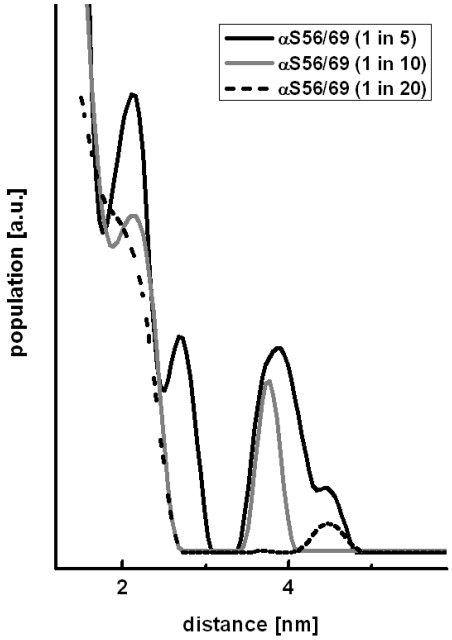

Figure 5.5 Distance distributions for the αS56/69 mutant with different diamagnetic dilutions.

5.4 Fibril fold model

Figure 5.6.a shows the schematic view of the protein in a plane perpendicular to the fibril axis as used in the model. In figure 5.6b the β-sheets are shown in a side view of the protein fibril. The mutants αS56/69, αS56/90, and αS69/90 provide a set of three intra-molecular distances that define the corners of a triangle in a plane perpendicular to the fibril axis (figure 5.6c). In a view along the fibril axis, the β-sheets appear as parallel strands. The triangle is rotated in the plane perpendicular to the fibril axis until each corner is as close as possible to one of the parallel strands. Thereby several orientations of the triangle are found. Arrangements in which residues are not sequential on successive parallel strands are excluded. We exclude these arrangements because such an arrangement would require that the protein exhibits too many turns for the distance. Also the solutions that involve residues on the same strand are excluded on the basis of the distances measured (table 5.1).

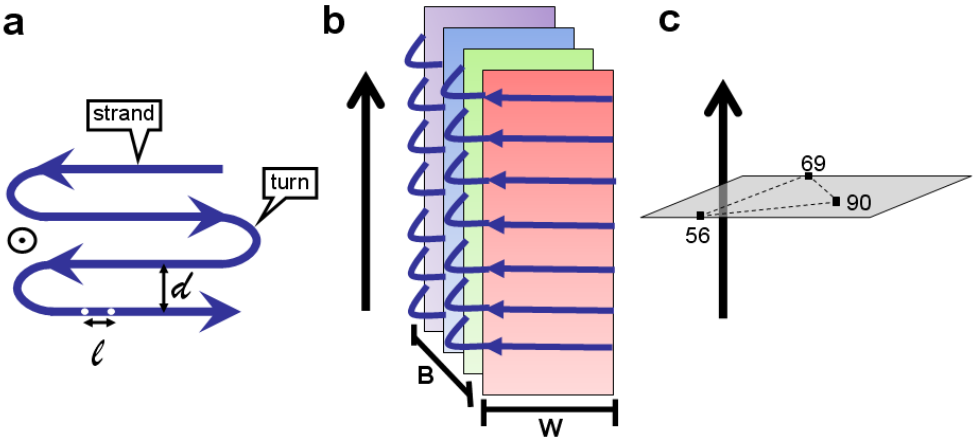

Figure 5.6 The cross-β-sheet structure of fibrils. a: View along fibril axis (fibril axis: black arrow that is pointing out of the page). Dark blue: protein. Strands and turns that connect the strands are labeled. *l*: distance between residues (dots) within the strand and *d*: distance between sheets. b: Fibril side view (fibril axis: black arrow), colored planes: β-sheets. Dark blue arrows: proteins making up the fibril. c: Location of residues 56, 69, and 90 assumed to make the model of the fibril.

Different spin-label linker orientations are considered to take the length of 0.5 nm from the protein C_β atom to the nitroxide group of the spin label into account (see materials and methods). We first describe the case in which all linkers point in the same direction. In total four solutions are found. In two of theses solutions, residues 56 and 69 or 69 and 90 are on the same strand. Consequently, these solutions are discarded. The remaining two solutions are equivalent but they reflect different threading of the protein through the points (compare figure 5.7a to b). Starting at residue 56, the protein can be threaded on strand II in the direction away from the position of 69 (figure 5.7a). In this case, turns at residues 58 to 62, 70 to 74, and 85 to 89 (residue i and residue i + 4) are predicted. If the protein sequence is threaded on strand II in the direction towards the position 69 rather than away from that, a turn involving residues 74 to 78 and a strand of two residues followed by a turn at residues 80 to 84 is predicted (figure 5.7b). This leaves a stretch of residues from 86 to 90 uncomplemented by an opposite β-sheet. This scenario seems unlikely, and is therefore discarded.

The other set of linker orientations produce solutions shown in figure 5.8, depicted as orange, pink, purple, and green dots. For the solutions shown in orange and pink all three linkers point towards the same side of their respective strand, e.g. towards strand I. A fibril model similar to figure 5.7 results, although with shifted turn

positions (figure 5.9). If the linkers at residues 69 and 90 point into a direction, which is opposite to that of residue 56, i.e., to the other side of their strand than 56, an alternative fold is possible (figure 5.10). The main difference is that there is only one turn between residues 69 and 90. This solution is possible for two sets of orientations of linkers (green and purple dots in figure 5.10). The two solutions in figure 5.10 result from the two ways of threading the protein through the points. In this scenario, a stack of three β-sheets between residues 56 and 90 would result. The complete protofibril from residue 38 to 90 would have three or four stacked β-sheets leading to a thickness B (figure 5.6b) of the protofibril of 2.18 nm respectively 3.27 nm, smaller than the dimension B of protofibrils (about 5 nm) [7]. Therefore, the fold shown in figure 5.10 is not reasonable.

Considering the distances reported by Karyagina et al. [8] we extended the model shown in figure 5.7a towards residue 41. The distance we measured for αS41/69 (3.1 nm, table 5.1) suggests that residue 41, on strand I, could be facing residues 56 or 57 on strand II, (figure 5.7a) thus yielding a distance between residues 41 and 69 of 2.8 nm or 3.0 nm, respectively. For those arrangements of residue 41, the predicted separation between residues 41 and 90 would be about 4 nm, in good agreement with the result of 4.5 ± 0.5 nm reported by Karyagina et al. [8]. A stack of five β-sheets would have a B value of 4.36 nm, in good agreement with predicted protofibril dimensions [7].

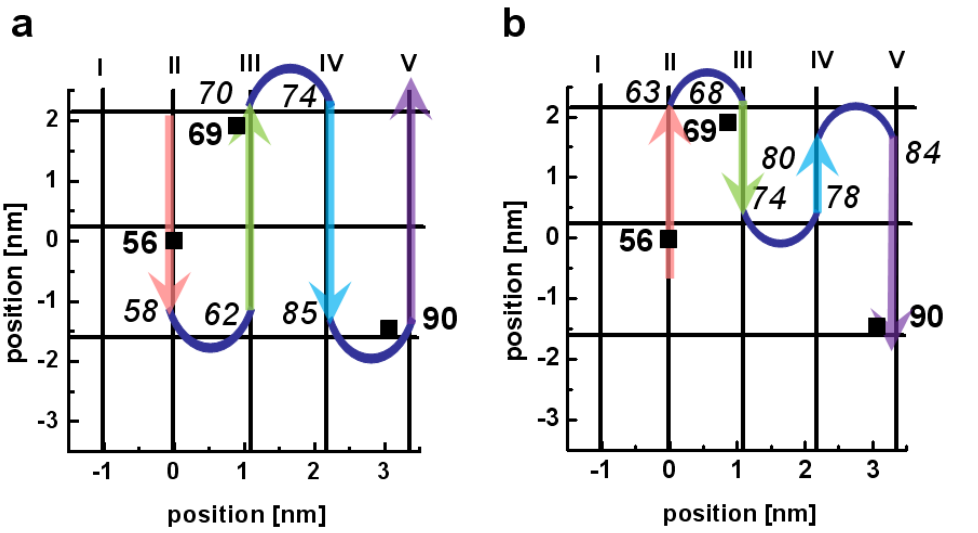

Figure 5.7 Models of the fold of αS in the fibril for all linkers pointing into the same direction. Strands are labeled I to V. Colored arrows indicate successive β sheets, and dark blue bent lines indicate turns. Italic numbers: residues at the start and the end of the turn. a: If the protein is threaded on strand II in the direction away from the position of 69, turns at residues 58 to 62, 70 to 74, and 85 to 89 are predicted. b: If the protein is threaded on strand II in the direction towards the position 69, a turn at residues 74 to 78 and a two-residue strand followed by a turn at residues 80 to 84 are predicted.

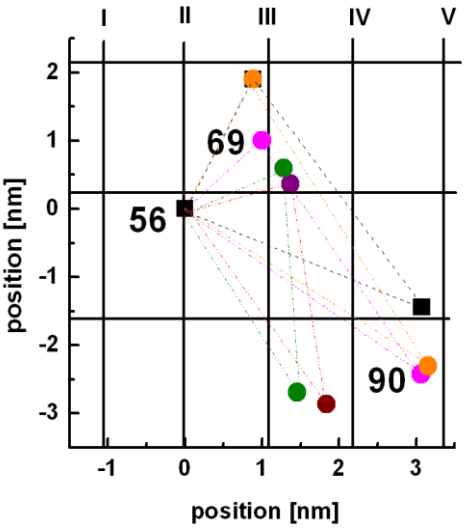

Figure 5.8 Effect of linker orientation on the position of residues 56, 69, and 90 with respect to the strands I to V. Dots in different colors show optimal positions found as acceptable solutions for the nine relative linker orientations. Lines joining positions (triangles) resulting for different linker orientations are given in the color used for the corresponding linker orientation. For details, see text.

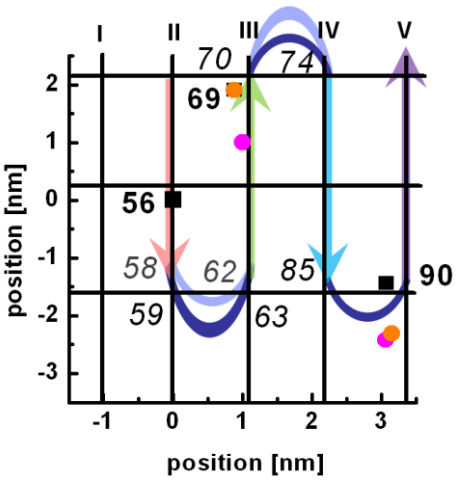

Figure 5.9 Effect of linker orientation on the model shown in figure 5.7.a. Pink and orange dots give the positions of residues 69 and 90 for two other orientations that are compatible with the fold obtained for parallel linkers. Orange dots show the position of residues if one or both linkers at 69 and 90 are almost parallel to the strand, but pointing towards the same side of the strands as the linker at residue 56. Black squares: positions shown in figure 5.7. The threading model is shown for the pink positions. Light-blue turns indicate the shift in the turn positions where strand IV is shifted by 2 residues relative to strand II, and turn positions differ by one (turn between strand II and III) and two residues (turn between strand IV and V). For position 69, the black square overlaps the orange dot.

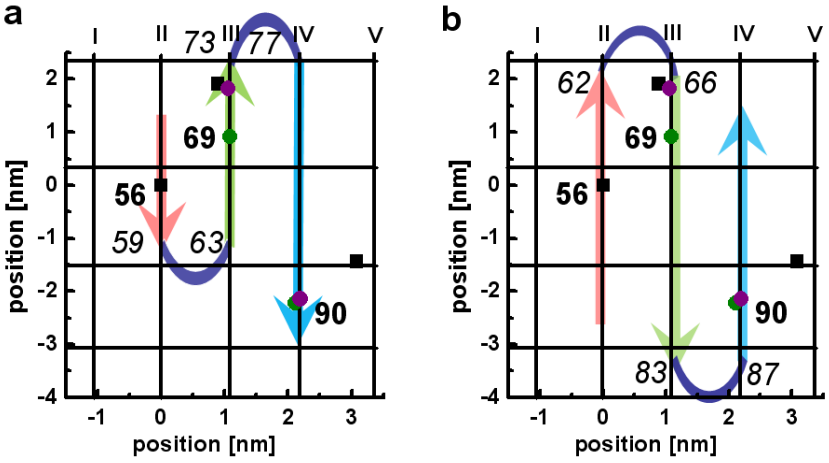

Figure 5.10 Alternative model of the αS fibril. a: Fold for linker orientations with the linker at residue 56 opposite to those at residues 69 and 90 for two different linker orientations (green and purple dots). b: Alternative way of threading the protein for the positions shown in a. The purple dot and the green dot labeled 69 are the alternative positions of residue 69. The black squares show the positions of residues 56, 69, and 90 in the model shown in figure 5.7.

5.5 Discussion

The morphology of the fibrils and the fibril growth are not affected by spin-label position or diamagnetic dilution as evidenced by the AFM and ThioT results. We therefore conclude that all mutants report on the same fibril morphology and that all distances can be used to derive a common model of the fold of the protein within the fibril. Fibrils of α-synuclein are in-register, parallel β-strand fibrils. Inter-molecular interactions of spin labels are therefore parallel to the fibril axis. This parallelism makes that inter-molecular distances reflect the inter-strand separation or multiples thereof and do not depend on the mutant, i.e., the residue of α-synuclein to which the spin label is attached. Therefore, inter-molecular distances identified from the diamagnetic-dilution series of αS56/69 are used also for the other double mutants. The best compromise between signal-to-noise and discrimination of intra- and inter-molecular distances is a diamagnetic dilution of 1 in 20.

For the mutants αS9/69, αS18/69, αS18/90, and αS27/56 one of the labeled positions is outside the region typically associated with the β-sheets of the αS fibrils, which ranges from residue 35-38 to 89-96 according to previous studies [4-7,19]. All these mutants, with the exception of αS27/56, have a majority population with distances longer than 5 nm (see results). This shows that the non-fibril, N-terminal part of αS at least up to residue 18 extends away from the fibril core. Residue 27 behaves differently. The mutant αS27/56 has a broad, continuous distance distribution, revealing that the region close to residue 27 is disordered. Distances of the αS27/56 mutant, which are extending from 2 to 4 nm, suggest that the region around residue 27 is closer to the fibril core than residues at the N-terminus around residue 18. The information obtained from the mutants αS9/69, αS18/69, αS18/90, and αS27/56 suggests the picture of an unstructured N-terminus that extends away from the fibril core.

The experimentally determined distances for αS56/69, αS69/90, αS56/90, and αS41/69 are significantly shorter than the distances expected for residues on the same strand (table 5.1). These experimentally determined distances reveal that there must be minimally one turn between residues 41 and 56, 56 and 69 and between 69 and 90, i.e., there are at least three turns separating residue 41 and 90. This leads to the picture that there are at least four strands of β-sheets, where the first strand contains residue 41 and the last residue 90.

The model described in section 5.4 shows how the distances can be converted to a picture of the fibril fold. We stress that this model derives from the present set of

constraints. To prove or disprove the model additional distance restraints would be needed.

The model of the fold of αS in the fibril (figure 5.7.a), derived from the situation in which all linkers are pointing into the same direction, suggests that the protofibril consists of five stacked β-sheets (I to V), spanning residues 41 (not directly determined, but inferred to be located on strand I) to 90. This model is also robust for a series of spin-label linker orientations, in which linkers are pointing into different directions. At most, extreme linker orientations shift strands with respect to each other, by up to three residues (figure 5.9). Nevertheless, there are linker orientations that could result in a fold in which the protofibril from residue 41 to 90 consists of four rather than five stacked β-sheets. In figure 5.10.a and b only three of these strands (residue 56 to 90) are shown. Such a model would disagree with the outside fibril dimensions and is therefore excluded.

Overall the fold shown in figure 5.10.a is similar to that proposed by Vilar et al. [7], in that three turns separate the strands containing residue 56 and 90. In this model, the first turn, 56-62 agrees with our results, whereas the second turn, 66-68 is four residues earlier in sequence, and thus suggests that there is an intervening strand between residues 56 and 69. Because this arrangement aligns residues 56 and 69 in a direction perpendicular to the strand, it would not violate the 56-69 distance constraint obtained in the present study. However, the model proposed by Vilar et al. would disagree with the distance we determine between residues 56 and 90, suggesting it to be longer than the distance between 69 and 90. The scenario of Vilar et al. [7] in which the distance between residues 56 and 90 is longer than the distance between of 69 and 90 is therefore not compatible with our data.

The model of Heise et al. [19], with turns at 65-69 and 82-87 again is compatible with the distance between 56 and 69, but not with the other distances.Unfortunately, the very recent model proposed by Comellas et al. [6], in which long and short β-strands alternate, cannot be checked against our data, because the overall arrangement of strands is not reported [6].

We show that a series of nine doubly labeled mutants of αS enables us to determine the fold of αS in the fibril, starting from the disordered N-terminus to the fibril core. We show that the N-terminus, presumably up to residue 27 is disordered and extends away from the fibril core. The β-sheet core from residue 41 to 90 comprises most likely five strands, leading to protofibril dimensions in agreement with previous results. This is the first step towards an atomic-resolution picture of the fibril core.

Reference List

[1] V. V. Shvadchak, L. J. Falomir-Lockhart, D. A. Yushchenko, T. M. Jovin, *J.Biol.Chem.* **2011,** *286* 13023-13032.
[2] K. A. Conway, J. D. Harper, P. T. Lansbury, Jr., *Biochemistry* **2000,** *39* 2552-2563.
[3] L. C. Serpell, J. Berriman, R. Jakes, M. Goedert, R. A. Crowther, *Proc.Natl.Acad.Sci.U.S.A* **2000,** *97* 4897-4902.
[4] M. Chen, M. Margittai, J. Chen, R. Langen, *J.Biol.Chem.* **2007,** *282* 24970-24979.
[5] A. Der-Sarkissian, C. C. Jao, J. Chen, R. Langen, *J.Biol.Chem.* **2003,** *278* 37530-37535.
[6] G. Comellas, L. R. Lemkau, A. J. Nieuwkoop, K. D. Kloepper, D. T. Ladror, R. Ebisu, W. S. Woods, A. S. Lipton, J. M. George, C. M. Rienstra, *J.Mol.Biol.* **2011,** *411* 881-895.
[7] M. Vilar, H. T. Chou, T. Luhrs, S. K. Maji, D. Riek-Loher, R. Verel, G. Manning, H. Stahlberg, R. Riek, *Proc.Natl.Acad.Sci.U.S.A* **2008,** *105* 8637-8642.
[8] I. Karyagina, S. Becker, K. Giller, D. Riedel, T. M. Jovin, C. Griesinger, M. Bennati, *Biophys.J.* **2011,** *101* L1-L3.
[9] M. E. van Raaij, I. M. Segers-Nolten, V. Subramaniam, *Biophys.J.* **2006,** *91* L96-L98.
[10] G. Veldhuis, I. Segers-Nolten, E. Ferlemann, V. Subramaniam, *Chembiochem* **2009,** *10* 436-439.
[11] M. Drescher, G. Veldhuis, B. D. van Rooijen, S. Milikisyants, V. Subramaniam, M. Huber, *J.Am.Chem.Soc.* **2008,** *130* 7796-7797.
[12] H. LeVine, III, *Protein Sci.* **1993,** *2* 404-410.
[13] H. Naiki, K. Higuchi, M. Hosokawa, T. Takeda, *Analytical Biochemistry* **1989,** *177* 244-249.
[14] K. O. Vanderwerf, C. A. J. Putman, B. G. Degrooth, F. B. Segerink, E. H. Schipper, N. F. Vanhulst, J. Greve, *Review of Scientific Instruments* **1993,** *64* 2892-2897.
[15] G. Jeschke, *Chemphyschem* **2002,** *3* 927-932.
[16] G. Jeschke, V. Chechik, P. Ionita, A. Godt, H. Zimmermann, J. Banham, C. R. Timmel, D. Hilger, H. Jung, *Applied Magnetic Resonance* **2006,** *30* 473-498.
[17] M. Margittai, R. Langen, *Q.Rev.Biophys.* **2008,** *41* 265-297.
[18] J. E. Banham, C. M. Baker, S. Ceola, I. J. Day, G. H. Grant, E. J. Groenen, C. T. Rodgers, G. Jeschke, C. R. Timmel, *J.Magn Reson.* **2008,** *191* 202-218.
[19] H. Heise, W. Hoyer, S. Becker, O. C. Andronesi, D. Riedel, M. Baldus, *Proc.Natl.Acad.Sci.U.S.A* **2005,** *102* 15871-15876.